Measurement of High Order X-point Magnetic Field Configurations in ASDEX Upgrade

Cian Roche
Supervisor - Mike Dunne

Department of Physics
University College Cork

ASDEX Upgrade
Institute of Plasma Physics

May 2018 - August 2018

ABSTRACT. Using poloidal flux matrices produced by CLISTE for various currents in the planned upper divertor control coils of ASDEX Upgrade, the magnetic field at each poloidal field probe was calculated and the theoretical magnetic measurement estimated. Predicted measurements were compared to that from various existing discharges to establish a typical error for a predicted measurement of roughly ± 1.5 mT. The simulated magnetic measurements were then examined, showing that that probes Bthe09-Bthe12 could most confidently detect the changes in the magnetic field for upper divertor control coil currents up to -50 kAt. It was also shown that regular magnetic field gradients cannot be assumed in the vicinity of control coils and so an average field must be calculated over the extent of each probe with a mesh spacing of 5×10^{-4} m or lower.

Typeset using LaTeX

1. Introduction

More complicated magnetic field structures near the upper divertor plates can "'flare out" the flux tubes, resulting in a power load distributed over an area roughly 2-3 times larger than the single null configuration (1). For this reason a set of control coils is planned for ASDEX Upgrade which will have a maximum operating current of 50 kAt (kilo Amp turns), allowing for more control over the magnetic field in the vessel. This control includes the position of and number of X-points, with the effect of these coils not limited to the high-Z (see next section for coordinate system) region of the vessel. A concern of ASDEX Upgrade is the confidence with which these new field configurations can be measured by the poloidal field coils. This project used CLISTE to produce poloidal flux matrices for various currents in the control coils and calculated theoretical magnetic measurements at each of the in-vessel probes to determine the viability of confidently measuring these new field configurations.

2. Background

2.1. Coordinates and sign conventions

It is first necessary to outline the coordinate system and conventions employed at ASDEX Upgrade. The coordinate system used is the cylindrical right-handed triplet (R, ϕ, Z) as in figure 1. Note the coordinate θ is also used, which is the angle in the poloidal plane. This angle is used to define the orientation of the probes (which is important as the field they measure is actually calculated via the rate of change of magnetic flux through the area defined by their loops) as shown in figure 2. The angle θ is measured CCW from the positive sense of the $\hat{R}$ axis when the origin is translated to r_i, the position of the i^{th} probe relative to the machine center.

2.2. Calculation of Magnetic Field from the Poloidal Flux

To calculate the magnetic field at some point in the poloidal plane, one first needs the derivatives of the poloidal flux Ψ in the R-Z plane. To explain this requires some background; the following is based a document entitled "Notes on tokamak Equilibrium" by Youjun Hu of the Institute of Plasma Physics, Chi-

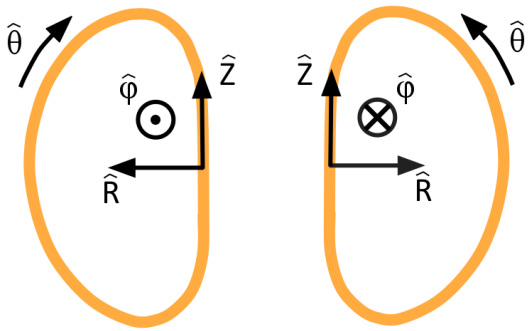

FIG. 1: *Coordinate system used at ASDEX Upgrade, where this view is a side-view of the torus. Note that the origin is actually at the machine center, so the high-field (closest to the center) side of the vessel is actually at* $R \simeq 1\ m$

nese Academy of Sciences.

Due to the divergenceless of the magnetic field, one can always write B as the curl of some magnetic vector potential[1], $\mathbf{A}(R,\phi,Z)$, ie $\mathbf{B} = \nabla \times \mathbf{A}$. Since we are concerned only with the (ideally) axially symmetric case of a tokamak, $\mathbf{B}$ and thus it's individual components must be independent of ϕ. It is easily shown that an axisymmetric vector potential $\mathbf{A}(R,Z)$ suffices to describe this magnetic field. Expanding this curl in the cylindrical coordinates employed here and omitting all ϕ derivatives of the components of $\mathbf{A}$ (since they must be zero) one obtains

$$\mathbf{B} = -\frac{\partial A_\phi}{\partial Z}\hat{\mathbf{R}} + \frac{1}{R}\frac{\partial (RA_\phi)}{\partial R}\hat{\mathbf{Z}} + \left(\frac{\partial A_R}{\partial Z} - \frac{\partial A_Z}{\partial R}\right)\hat{\phi} \tag{1}$$

Now, looking only at the poloidal ((R,Z) plane) components, it is possible to write these components in terms of a new function we'll call $\psi(R,Z)$, the physical meaning of which will become apparent soon. This function is defined as $\psi(R,Z) = RA_\phi(R,Z)$, with the poloidal components now expressed as

[1] For a detailed explanation, see Griffith's Electrodynamics or any introductory electrodynamics text

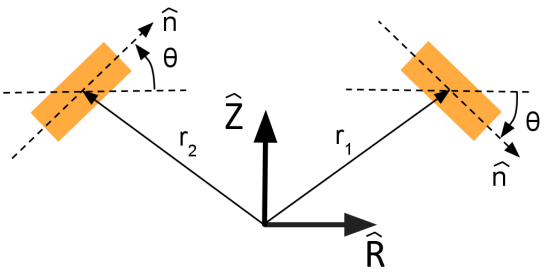

FIG. 2: *Two examples of probe orientation, both on the right hand side of the vessel (right hand side of figure 1). On the left, θ is positive. On the right, θ is negative. Note that $\hat{n}$ is the normal to the open surfaces defined by the loops.*

$$B_R = -\frac{1}{R}\frac{\partial \psi}{\partial Z} \qquad B_Z = \frac{1}{R}\frac{\partial \psi}{\partial R} \tag{2}$$

To find out what this ψ means physically, we have a look at a poloidal cross section with two magnetic surfaces labelled (Fig. 3). (A magnetic surface being, at least in this ϕ symmetric case, the surface of revolution obtained by rotating the projection of a magnetic field line on the (R,Z) plane around the Z axis. Perhaps more illuminating is the fact that along a magnetic field line, Ψ is constant, ie $d\Psi = 0$.) Why are we looking at magnetic surfaces? Well it turns out (as shown below) that magnetic surfaces are exactly the contours of ψ on the (R,Z) plane. Remembering that on a contour of a function f the change in f is zero, ie $df = 0$, then on a contour of ψ:

$$\begin{gathered} d\psi = 0 \\ \Rightarrow \frac{\partial \psi}{\partial R} dR + \frac{\partial \psi}{\partial Z} dZ = 0 \end{gathered} \tag{3}$$

Via the chain rule. This can be recast using our expressions for B_R and B_Z by first multiplying across by $1/R$, yielding:

$$\begin{gathered} B_Z dR - B_R dZ = 0 \\ \frac{dZ}{dR} = \frac{B_Z}{B_R} \end{gathered} \tag{4}$$

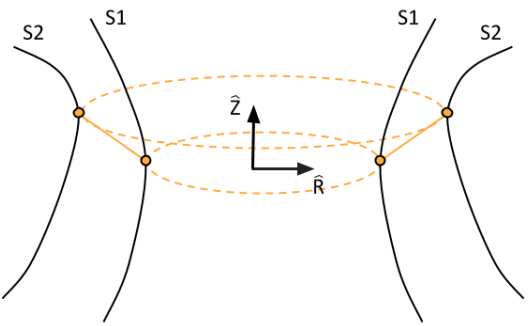

FIG. 3: *Poloidal cross section of two magnetic surfaces (thus, contours of ψ as explained here) $S1$ and $S2$*

Equation 4 is actually the equation of the projection of a magnetic field line on the (R,Z) plane. (Note that along a magnetic field line the constant quantity is the magnetic flux, ie $d\Psi = 0$). Thus, we have shown that the equation of a contour of ψ can be expressed as that of a magnetic surface. In other words, the contours of ψ on the (R,Z) plane are the previously defined magnetic surfaces. We now use this knowledge in the example of Fig. 3.

Evidently the lines labelled $S1$ and $S2$ are only "slices" of the full surfaces, but imagine the full surfaces defined by the rotation of these lines around the Z axis. Note that since magnetic monopoles don't exist, magnetic field lines are closed[2] and thus to draw the diagram in full would require completing the loops of $S1$ and $S2$ such that they form two sets nested loops in the (R,Z) plane. Taking any toroidal ribbon, (by choosing a point on $S1$ and also on $S2$, connecting them and rotating this line segment around Z, one obtains a "ribbon") we calculate the poloidal magnetic flux $\Psi_{B,pol}$ through this surface (which is enclosed by the two segmented orange lines in Fig. 3) as

$$\Psi_{B,pol} = \iint_{\text{ribbon}} \mathbf{B_{pol}} \cdot d\mathbf{a}$$

However, we can exploit Gauss' theorem in the volume between $S1$ and $S2$,

[2] For an in depth discussion of the history of the magnetic monopole, see Chapter 1 in D.C. Mattis, The Theory of Magnetism (New York: Harper Row, 1965).

as since the boundary values are the same for any such defined toroidal ribbon, we can choose a simplifying case and obtain the same answer. So we choose a ribbon parallel to the R axis (ie only the Z component of the poloidal magnetic flux is non-zero) such that the point on $S1$ is at (R_1, Z) and the point on $S2$ is at (R_2, Z). With $\hat{\mathbf{Z}}$ as the positive direction for the surface normal, we have:

$$\begin{aligned}
\Psi_{B,pol} &= \int_{R_1}^{R_2} \int_0^{2\pi} B_Z(R,Z) d\mathbf{a} \\
&= \int_{R_1}^{R_2} B_Z 2\pi R dR \\
&= \int_{R_1}^{R_2} \frac{1}{R} \frac{\partial \psi}{\partial R} 2\pi R dR \\
&= 2\pi \int_{R_1}^{R_2} \frac{\partial \psi}{\partial R} dR \\
\Psi_{B,pol} &= 2\pi \left[\psi(R_2) - \psi(R_1)\right] \qquad (5)
\end{aligned}$$

Just like that we have discovered a physical correspondence for the function ψ. The poloidal magnetic flux between two magnetic surfaces is simply 2π (because it runs around the complete azimuthal range) times the difference of ψ between these magnetic surfaces. This is why ψ is called the "poloidal flux function", as it's difference between two points is directly related to the poloidal flux through any surface with boundaries on the magnetic surfaces on which the points lie.

The poloidal flux function is thus in some ways (although not strictly accurate) the physical poloidal flux per radian. This relationship allows for the magnetic components B_R and B_Z to be rewritten in terms of the physical poloidal magnetic flux $\Psi_{B,pol}$ (subscripts omitted) as:

$$B_R = -\frac{1}{2\pi R} \frac{\partial \Psi}{\partial Z} \qquad B_Z = \frac{1}{2\pi R} \frac{\partial \Psi}{\partial R} \qquad (6)$$

Another, simpler way to come to this conclusion is to recognise that $B = d\Psi/dA$, and so using two different surfaces we can easily obtain B_R and B_Z. First, consider a toroidal strip with normal only in $\hat{\mathbf{Z}}$ (ie no flux through it due to B_R). The strip has thickness dR (the thickness is colinear with $\hat{\mathbf{R}}$) at radial

distance R with area element $dA = 2\pi R dR$ (the well-known and easily derived area element of a ring). This toroidal strip has only poloidal flux due to B_Z, and so we can calculate this easily as (note partial derivative because $\Psi = \Psi(R,Z)$)

$$B_Z = \frac{d\Psi}{dA} = \frac{1}{2\pi R}\frac{\partial \Psi}{\partial R} \tag{7}$$

Similarly, if we consider a toroidal strip which has normal only in $\hat{\mathbf{R}}$ such that the only flux contribution is from B_R, and the strip has thickness dZ colinear with $\hat{\mathbf{Z}}$, we can calculate B_R. Now $dA = 2\pi R dZ$, but this this time the normal is anti-aligned with $\hat{\mathbf{R}}$ (ie points in -$\hat{\mathbf{R}}$) as opposed to the previous case in which $\hat{\mathbf{n}}$ pointed along $\hat{\mathbf{Z}}$.

$$B_R = \frac{d\Psi}{dA} = -\frac{1}{2\pi R}\frac{\partial \Psi}{\partial Z} \tag{8}$$

3. Effect of Probe Properties on Measured Quantities

3.1. Probe angle

The poloidal field probes of ASDEX Upgrade measure the time rate of change of magnetic flux through their area, then digitally integrate this signal to obtain a magnetic field time series. Since this measurement is based on magnetic flux through the coils of the probe, the angle of the probe in the poloidal plane will alter the measurement. With all notation and conventions as in figure 1, the theoretically calculated component of both B_R and B_Z which are perpendicular to $\hat{\mathbf{n}}$ must be discounted. In other words, only their components parallel to $\hat{\mathbf{n}}$ would actually be measured.

Reminder of the task: Remember that first, CLISTE produces a matrix of poloidal flux values given property profiles for the plasma. This flux matrix can then be used to calculate a theoretical estimate for the magnetic field (both components) at any point in the poloidal plane via Equation(s) 6. These calculations must then be adjusted to take into account the fact that the probes of the machine are at different angles and will not measure the “total” field.

Via simple trigonometry, the component of B_R which is parallel to $\hat{\mathbf{n}}$ is $B_R \cos\theta$, whereas the component of B_Z parallel to $\hat{\mathbf{n}}$ is $B_Z \sin\theta$. Thus the predicted measurement (with B_R and B_Z already calculated via Equation(s) 6) is given by

$$B_{\text{meas}} = B_R \cos\theta + B_Z \sin\theta \tag{9}$$

3.2. Impact of Probe Extent

The extent of the probe will also affect measurements, in that the field at one end of the probe will likely differ from the field at the other end, so to be perfectly accurate the measurements at each point in the volume of the probe would have to be averaged. A demonstration of the variation of the magnetic field over the extent of a probe is shown in Figures 4(a) and 4(b). In Figure 4(a) is a probe over which the field varies at a roughly constant rate, appearing as a plane. In this case, the average value over the extent of the probe almost exactly matches the central value. In Figure 4(b) is a case in which the field does not vary uniformly and thus the average value is not well approximated by the central value.

A further, more quantitative demonstration of the impact of extent on the measurements is shown in Figure 5 for the 40 Bthe probes. This represents the difference between the center value an average value (calculated over 2500 mesh points) for each probe for two magnetic field configurations: The first in which the upper divertor coil current is zero and a second comparison in which the upper divertor coils have a current of -50 kAt (the maximum operational current for the upper control coils). Probes closest to the control coils have the most irregular gradients of the magnetic field and thus the center value does not accurately represent the probe measurement. For the upper divertor control coils, the closest probes are in the range of roughly Bthe09 to Bthe12 and their central values diverge greatly from the average value (and therefore the actual measurement). The maximum deviation occurs for Bthe12 in this case with a magnitude of roughly 7.5 mT, about 5 times the typical error of CLISTE probe measurement predictions.

In order to accurately predict probe measurements (ie to avoid typical errors away from the upper control coils of between 0.5 and 1 mT, and errors up to 8

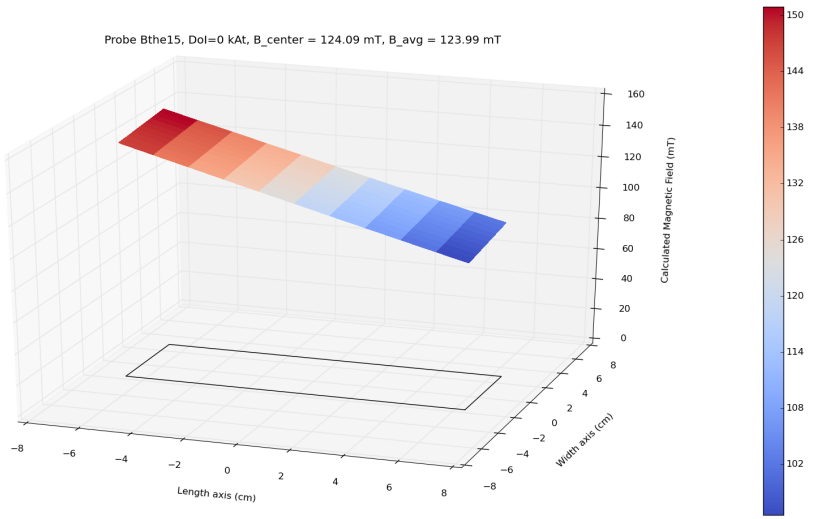

(a) Regular variation of B

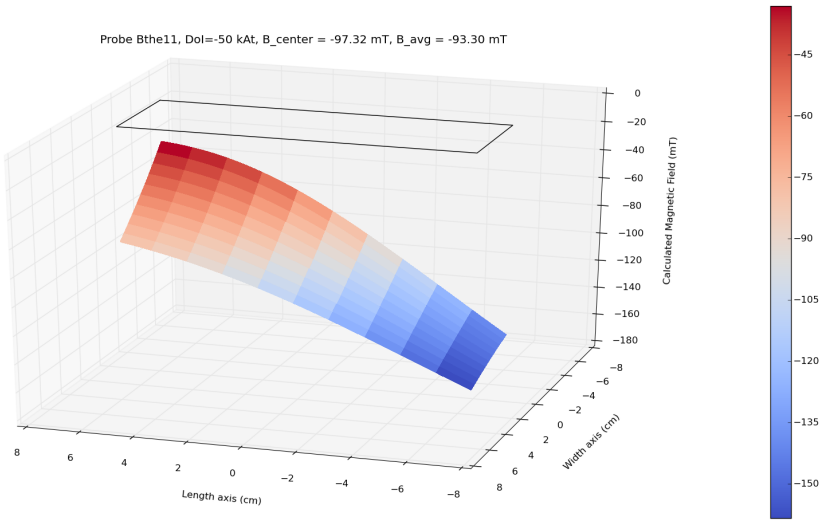

(b) Irregular variation of B

FIG. 4: *Variation in calculated magnetic field over the extent of two example probes. Note that in (b) there is a current present in the planned upper divertor coils which increases irregularity*

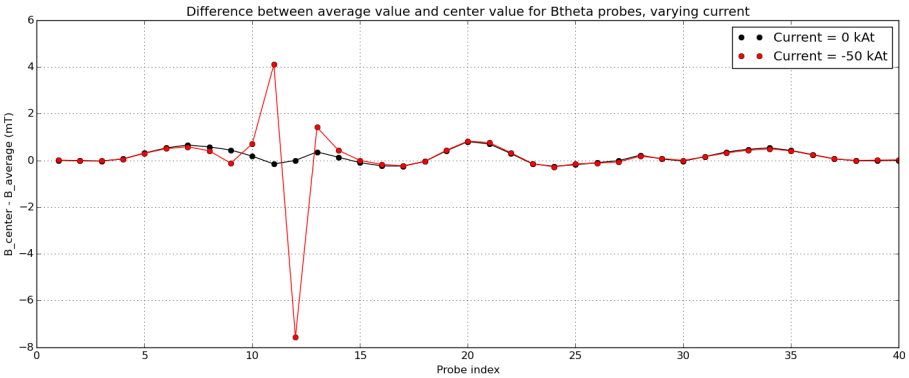

FIG. 5: *Average magnetic field value over a probe calculated here using a 50×50 grid of points over the extent of each probe.*

mT near these coils) particularly in the case of high upper divertor control coil currents, the average field over the extent of the probe must be calculated as the assumption of a regular gradient breaks down.

3.3. Spatial resolution

The spatial resolution with which the average value is calculated is important, as the calculated average varies greatly for mesh spacing on the order of 0.5 - 1.0 cm as shown in Figure 6 for the three probes with largest deviation from their central value. Clearly any mesh spacing above 1 mm is unreliable as small changes in this quantity result in variation of the average value on the order of 0.5 mT. Saturation occurs for mesh spacings below 1mm, although it is worth noting that the number of calculations to obtain an average field is inverse-square proportional to this grid spacing (ie for a 10x10 grid 100 calculations are required, but if the spacing is decreased by a factor of 10 so that the grid is now 100x100, 10,000 calculations are required).

For this reason as the grid spacing approaches 10^{-4} m, the computational time becomes quite large. The dimensions of the Bthe probes are 0.131 m $\times$ 0.045 m, meaning a grid spacing of 10^{-4} m corresponds to an evenly-spaced

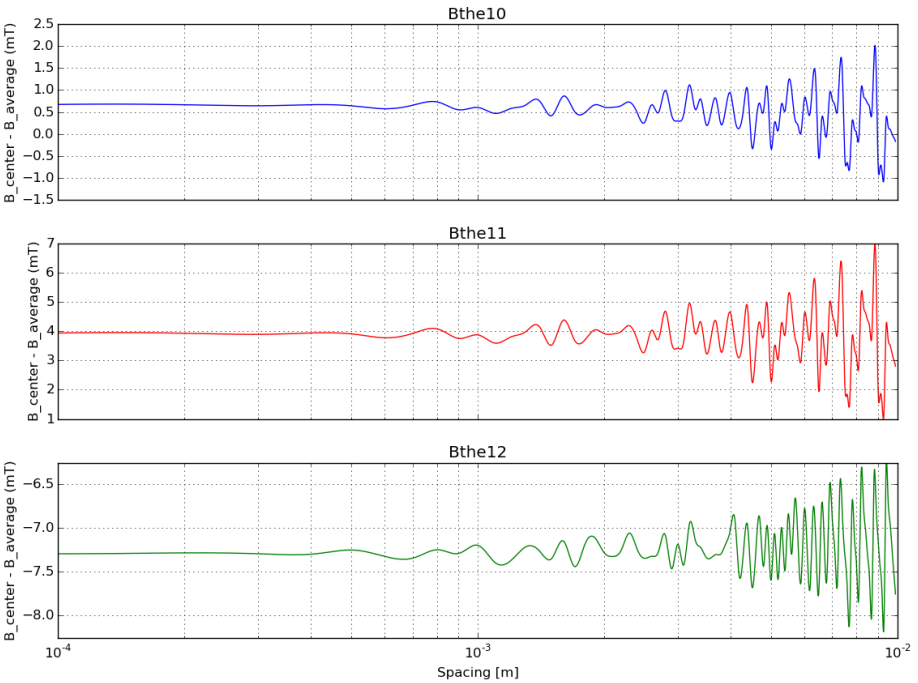

FIG. 6: *Difference between center value and average value for maximum upper divertor coil current (-50 kAt) as a function of the probe extent mesh grid spacing. Equal spacing is used along the length and width axes of the probe. The three probes shown here are those most affected by the upper control coils.*

mesh of 1310×450 points. This is a total of about 590,000 calculations of the magnetic field via equations 6 for each probe, whereas for a mesh spacing of 10^{-3} m, this is reduced to 5,900 calculations. Taking this into account, the most reasonable grid spacing appears to be 5×10^{-4} m, as this is in the region of saturation and requires $262 \times 90 \simeq 24,000$ calculations, a factor of 25 lower than that for a mesh spacing of 10^{-4} m. Even with much less calculations, the results obtained for a mesh spacing of 5×10^{-4} are consistently within 0.1 mT of that for a spacing of 10^{-4}. Note that 0.1 mT is an order of magnitude smaller than the typical random noise of the measurements.

3.4. Irregularity near Bthe20

Not only the probes close to the upper divertor control coils are poorly approximated by their center value. For example probe Bthe20 experiences a deviation of roughly 1 mT from the center value, with the difference decreasing moving away from this probe location. This is due to the presence of ferromagnetic plates in the vessel very close to Bthe20, as when plasma is present small currents are induced in the plates that locally distort the magnetic field. For the example discharge used here (shot number 34263) a demonstration of this local distortion is shown in Figure 7. Shown is the poloidal flux matrix contour plot created by CLISTE first without accounting for the effects of magnetization due to the 7 ferrite tiles along the inner limiter (represented by the green contour), then with these tiles present.

Clearly the contours become warped or "wavy" when the local distortions are taken into account. This corresponds to irregularities in the magnetic field which decrease the accuracy of the assumption of regular poloidal flux gradient. As expected, by moving away from these plates their effect is reduced, which is why probes 18 and 23 are largely unaffected. The order of this error is up to 1 mT, which can be avoided by averaging over the probe or by accounting for the tiles in CLISTE.

3.5. Calculation of average field over probe extent

Now that it is clear an average field must be calculated, it is useful to outline how this is calculated for a general probe i with center at (R_i, Z_i) in the (R,Z) plane, at a poloidal plane angle of θ_i as in figure 1. First we define a second orthogonal coordinate system (x,y) shown in Figure 8 in which $\hat{\mathbf{x}}$ points along $\hat{\mathbf{n}}$ (ie the "length" axis) and $\hat{\mathbf{y}}$ points along the width axis of the probe. Note that the origin is at the probe center (ie at position (R_i, Z_i) in the (R,Z) coordinate system) and this new coordinate system changes for each probe.

To obtain a mesh of points over the extent of the probe is not easy in the (R,Z) coordinate system, but is very simple in (x,y). Therefore we first create a mesh in (x,y) using $x \in [-l/2, l/2]$, $y \in [-w/2, w/2]$ where l and w are the length and width of the probe, respectively. We then need to calculate the mag-

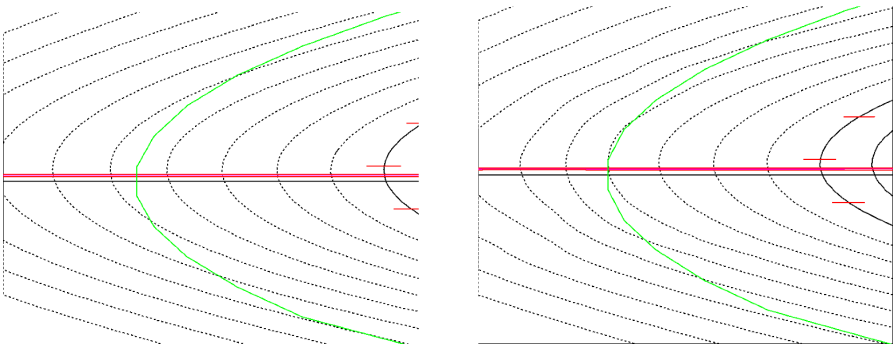

(a) Regular variation of B (b) Irregular variation of B

FIG. 7: *The plots show a 1 metre high ($Z \in [-0.5, 0.5]$ m) by 10 cm wide ($R \in [1.0, 1.1]$ m) section of CLISTE equilibrium (34263, t=3.5 sec) poloidal flux contours. The horizontal axis is greatly stretched (greater than a factor of 10) to highlight the differences between the smooth contours in the 1st plot and the distortions of some contours in the 2nd plot, particularly in the top left quadrant of the 2nd plot. This region partially overlaps the volume occupied by the Bthe20 magnetic probe (coordinates of centroid: R = 0.98 m, Z= +0.159 m). Courtesy of P. J. McCarthy*

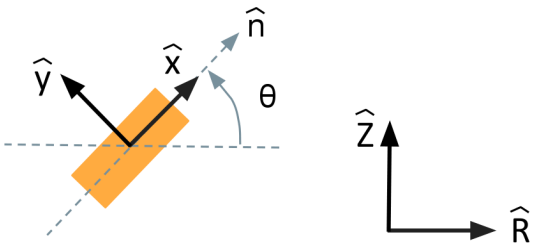

FIG. 8: *Secondary coordinate system for calculating the magnetic field over the extent of a general probe.*

netic field at each point on this grid, but the calculation is in terms of R and Z, so for each point we must first convert it to the (R,Z) coordinate system and then perform the calculation.

To transform from the (x,y) to the (R,Z) coordinate system is quite simple and well known (temporarily ignoring the translation of the origin) given that (x,y) is just rotated CCW by an angle θ_i relative to (R,Z). This is equivalent to saying (R,Z) is just rotated CCW by an angle $-\theta_i$ relative to (x,y), so we make use of the well known result of the transformation of a vector (ie a point) from one coordinate system to another which is rotated CCW by an angle θ relative to the first (but here we use $-\theta_i$). Here our "original" coordinate system is (x,y) with coordinates of a general point (x',y') and our "new" coordinate system is (R,Z) with coordinates (R',Z'). To obtain (R',Z') given (x',y'),

$$\begin{bmatrix} R' \\ Z' \end{bmatrix} = \begin{bmatrix} \cos\theta_i & -\sin\theta_i \\ \sin\theta_i & \cos\theta_i \end{bmatrix} \begin{bmatrix} x' \\ y' \end{bmatrix} = \begin{bmatrix} x'\cos\theta_i - y'\sin\theta_i \\ x'\sin\theta_i + y'\cos\theta_i \end{bmatrix}$$

Now, if the origin of both coordinate systems were in the same place we would be finished, but the (x,y) coordinate system is translated to the position of the center of the i^{th} probe, (R_i,Z_i). To account for this, the coordinates of a point (x',y') in our meshgrid in the (R,Z) coordinate system (which we will call (R^*,Z^*) here) are the rotated coordinates (R',Z') added to the the coordinates of the center (R_i,Z_i). ie

$$\begin{bmatrix} R^* \\ Z^* \end{bmatrix} = \begin{bmatrix} R_i + x'\cos\theta_i - y'\sin\theta_i \\ Z_i + x'\sin\theta_i + y'\cos\theta_i \end{bmatrix}$$

Put simply, the coordinates of any point in the grid over the probe can be expressed in terms of the position of the center of the probe, plus a displacement in each direction relative to the center of that probe. These coordinates (R^*,Z^*) are those used in the calculation of the magnetic field at each grid point via equation(s) 6.

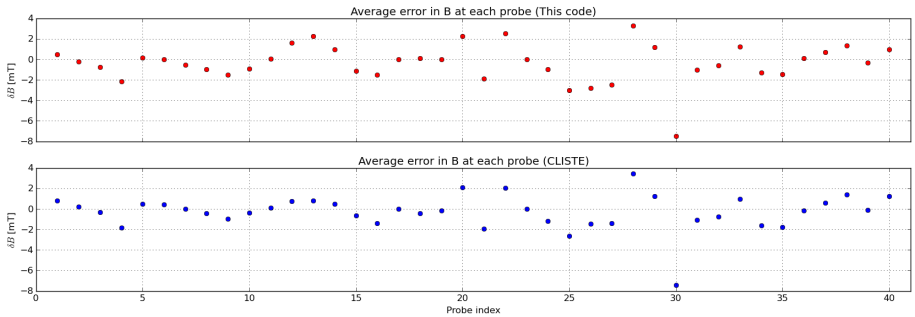

FIG. 9: *A comparison of the accuracy of the code used here and the results of CLISTE for the 40 Bthe probes of ASDEX Upgrade averaged over many discharges.*

4. Accuracy of Predicted Measurements

4.1. Comparison to magnetic measurements

By calculating the predicted magnetic measurements (with the python scripts written for this project) for many discharges and comparing them to the measured values, a typical error can be estimated for each poloidal field probe. This was also completed for the CLISTE results to compare the accuracy of both methods. When looking at a single discharge, the difference between the CLISTE values and this code's values can be up to 5 mT (although typically much smaller), but as shown in Figure 9, when averaged over many discharges their predictions are almost identical.

What is particularly interesting about this average error is that the probes Bthe30 and Bthe28 are, on average, the least accurate. Not only this but their standard deviations are much higher than that for the other probes as shown in Figure 10; this plot represents the change in measurement at each poloidal fied probe when the maximum UDC current is present (at this moment, -50 kAt) relative to zero current in these coils. The error bars are 1σ standard deviations, calculated using the error in predicted measurement for many discharges for each probe. Note that in future plots, the error bars are increased to 2σ.

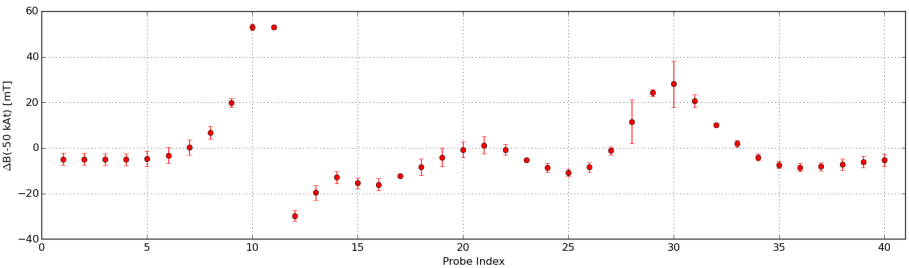

FIG. 10: *Change in probe measurements* $\Delta B(-50\ kAt) = B_{calc}(-50) - B_{calc}(0)$ *ie* $\Delta B(-50)$ *is the change in B at each probe going from 0 current to -50 kAt in the UD coils. Poloidal flux matrices produced by CLISTE in interpretive mode.*

Clearly the probes which experience the greatest change in measurement are those close to the upper divertor (probes 9-12) which are at high Z, but interestingly the probes at low Z (probes 28-32) also experience a large change in measurement. Ideally, both sets of coils coils be very useful for detecting new magnetic field configurations, but as was mentioned probes 28 and 30 are very unreliable. The reason for this is currently unknown, but the issue is being addressed. Thus, the primary (reliable) tools in measuring new magnetic field configurations due to current in the UDCs are unsurprisingly the probes closest to these coils. The errors associated with probes 9-12 are very low, at up to 1.5 mT for this code's predictions, and up to 1 mT for CLISTE's predictions, which is only $\sim 3\%$ of the change in measurement at probe 10/11 due to the maximum current in the UDCs.

5. Probe Measurements for Various UDC Currents

In the previous section, the case of maximum UDC current was used for demonstration as it resulted in the largest change in magnetic field measurements, but in this section the probe measurements at varying UDC currents are compared. A metric for the confidence with which the magnetic field configurations are measured is given by the ΔB plots in which 2σ error bars depict the uncertainty in these predictions. Both probes Bthe30 and Bthe28 are considered outliers for this discussion.

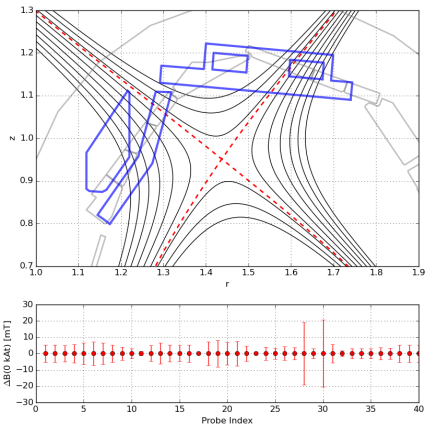

(a) No UDC current

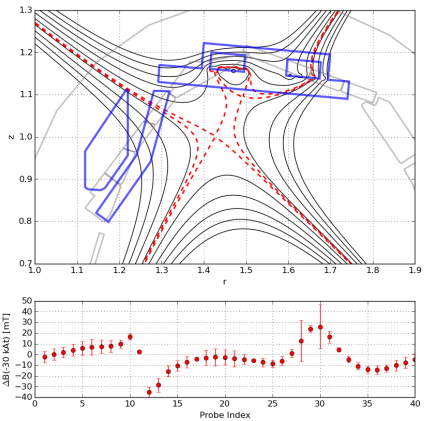

(b) UDC current of -30 kAt

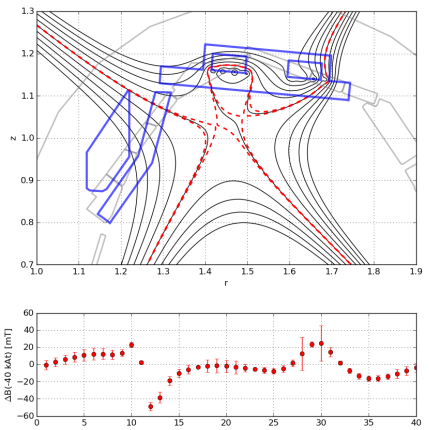

(c) UDC current of -40 kAt

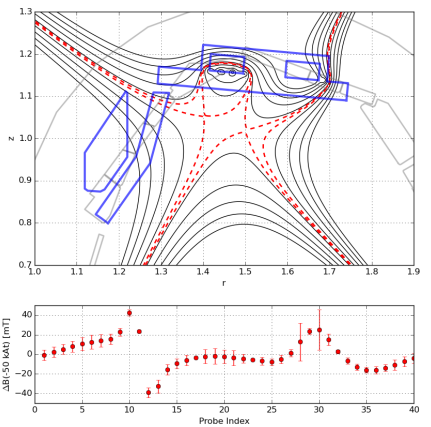

(d) UDC current of -50 kAt

FIG. 11: *Contours of the poloidal flux for various UDC currents, with the difference in measurement at each poloidal field probe relative to the 0 current case shown beneath each contour plot. Contour plot axes in [m], separatrices (contours which contain nulls) in dashed red. Current vessel components in grey, planned components in blue. In black are 9 evenly spaced contours in the range of [-1.675,-1.5] inclusive.*

Clearly Figure 11 demonstrates that the magnitude of the change in measurement for each UDC current shown is far above even the 2σ error in prediction for those poloidal field probes in the vicinity of these planned coils. Even in the case of probes far from the UDCs, many of the measurements (particularly those at low-Z) are still very confidently predicted relative to 0 UDC current.

6. Future Work

The next steps for this project could be as follows. Firstly, More magnetic field configurations should be investigated based on the outputs of CLISTE for various UDC currents, with more attention paid to the probes which cannot be relied upon when attempting to reproduce these field configurations. Secondly, the output probe measurements need to be run back through CLISTE and the differences between the original flux matrix used to produce these measurements and the flux matrix produced *using* these measurements examined; this will test the robustness of the predictions. Finally to properly determine the confidence with which these magnetic field configurations can be measured/ these measurements predicted, the random Gaussian noise of the probe measurements must be taken into account. Additive Gaussian noise on the order of 1 mT has been shown by Padraig Mac Carthaigh to be appropriate for this, which is easily implemented.

References

[1] Physics of Plasmas 15, 092501 (2008); doi: 10.1063/1.2967900

[2] Introduction to electrodynamics - David J. Griffiths

[3] The Theory of Magnetism - D.C. Mattis